



HAL
open science

Ultra-high-reflectivity photonic-bandgap mirrors in a ridge SOI waveguide

Philippe Velha, Jean-Claude Rodier, Philippe Lalanne, Jean-Paul Hugonin, D. Peyrade, E. Picard, T. Charvolin, E. Hadji

► **To cite this version:**

Philippe Velha, Jean-Claude Rodier, Philippe Lalanne, Jean-Paul Hugonin, D. Peyrade, et al.. Ultra-high-reflectivity photonic-bandgap mirrors in a ridge SOI waveguide. *New Journal of Physics*, 2006, 8, pp.204. 10.1088/1367-2630/8/9/204 . hal-00394753

HAL Id: hal-00394753

<https://hal.science/hal-00394753>

Submitted on 11 Apr 2016

HAL is a multi-disciplinary open access archive for the deposit and dissemination of scientific research documents, whether they are published or not. The documents may come from teaching and research institutions in France or abroad, or from public or private research centers.

L'archive ouverte pluridisciplinaire **HAL**, est destinée au dépôt et à la diffusion de documents scientifiques de niveau recherche, publiés ou non, émanant des établissements d'enseignement et de recherche français ou étrangers, des laboratoires publics ou privés.

Ultra-high-reflectivity photonic-bandgap mirrors in a ridge SOI waveguide

This content has been downloaded from IOPscience. Please scroll down to see the full text.

2006 New J. Phys. 8 204

(<http://iopscience.iop.org/1367-2630/8/9/204>)

View [the table of contents for this issue](#), or go to the [journal homepage](#) for more

Download details:

IP Address: 129.104.29.2

This content was downloaded on 02/11/2015 at 10:36

Please note that [terms and conditions apply](#).

Ultra-high-reflectivity photonic-bandgap mirrors in a ridge SOI waveguide

P Velha^{1,2,3}, J C Rodier¹, P Lalanne¹, J P Hugonin¹, D Peyrade²,
E Picard³, T Charvolin³ and E Hadji³

¹ Laboratoire Charles Fabry de l'Institut d'Optique, Centre National de la Recherche Scientifique, Université Paris XI, 91 403 Orsay Cedex, France

² Laboratoire des Technologies de la Microélectronique, Centre National de la Recherche Scientifique, UMR5129, 17, rue des Martyrs, 38054 Grenoble Cedex 9, France

³ Laboratoire Silicium Nanoélectronique Photonique et Structure, Département de Recherche Fondamentale sur la Matière Condensée, Commissariat à l'Energie Atomique, 17 rue des Martyrs, F-38054 Grenoble Cedex, France
E-mail: philippe.lalanne@iota.u-psud.fr

New Journal of Physics **8** (2006) 204

Received 6 April 2006

Published 22 September 2006

Online at <http://www.njp.org/>

doi:10.1088/1367-2630/8/9/204

Abstract. Microcavities consisting of two identical tapered mirrors etched into silicon-on-insulator ridge waveguides are investigated for operation at telecommunication wavelengths. They offer very small modal volumes of approximately $0.6 (\lambda/n)^3$ and calculated intrinsic Q factors of 400000. We have measured a Q factor of 8900 for a loaded cavity, in agreement with the theoretical value. In contrast to recent works performed on suspended membranes, the buried SiO_2 layer is not removed. The cavities possess strong mechanical robustness, thus making them attractive from the viewpoint of integration in large systems. The cavity Q factor is much larger than those previously obtained for similar geometries on a substrate.

Contents

1. Introduction	2
2. Design considerations	4
3. Experimental results	8
4. Conclusion	11
Acknowledgments	12
References	12

1. Introduction

In recent years, the race for faster optical communication and data processing has motivated research towards optoelectronic devices with more functional elements directly interconnected on a single chip to truly integrated circuits [1]. High- Q optical microcavities which confine light in volumes V of optical-wavelength scales are essential components for signal processing functions, including channel-drop filtering, on-off switching, light modulation and for exaltation of optical nonlinearities. From a more fundamental point of view, optical microcavities are currently investigated for spontaneous-emission inhibition or enhancement [2] or threshold laser reduction [3] for instance.

Recently, there has been an explosion of interest in manufacturing ultrasmall microcavities with extremely high- Q factors. Major achievements have been obtained over the past few years. For instance, the mode volume of toroid microcavities [4] on-a-chip has been reduced by two orders of magnitude, while preserving record Q values in the range of 10^8 . Similarly, technology has recently boosted the fabrication of GaAs/AlAs micropillar cavities [5] with pillar diameters close to 400 nm, and with smooth, straight, and vertical sidewalls, as attested by the high- Q reported in excess of 2000. Microcavities in two-dimensional photonic-crystal (PC) slabs, which offer mode volumes close to the theoretical limit $V = (\lambda/2n)^3$ have also been boosted, and Q factors almost as high as 10^6 are now available in several research laboratories [6]. Interpreting the light confinement in those PC cavities with a classical Fabry-Perot model, in which a guided Bloch mode is bouncing in PC waveguide closed at both extremities by two PC mirrors [7], implies that modal reflectivities for the Bloch mode are in excess of $R = 0.99998$. Such a high reflectivity represents an impressive value which is currently out of reach of the well-mastered thin-film approach even with up-to-date automated deposition techniques. It is perhaps the first time that high-reflectors relying on standard lithography processes have been manufactured with performance in excess of those achieved by multilayer high-reflectance coatings. However, let us note that in thin films coatings, one is currently concerned with controlling uniformity and roughness on cm^2 scales, while the PC high-reflectors are dealing with guided modes with μm^2 cross-sections.

These record reflectance values have been achieved in semiconductor membrane in air. Even though suspended membranes are viable at a research level, their prospects as basic building blocks for integrated optical device are clouded by several issues. Efficient current injection is difficult and has to be provided laterally. Not only is air an electrical insulator, it is also a thermal insulator. For nonlinear applications where high power density is required, concern is raised

for suspended membranes as to whether they are capable of channelling the heat. Finally the mechanical robustness of suspended membranes is questionable, particularly for devices with large dimensions. All this represents an obstacle from the viewpoint of practical applications, and realizing ultra-small high- Q cavities on a substrate represents a critical issue. This is not a straightforward task. For instance, as shown in a recent report [8], three missing-hole PC cavities with Q values in excess of 5000 in a suspended silicon membrane offer Q values 10 times smaller once implemented without removing the sacrificial buried SiO₂ layer.

In this work, we address the problem of designing short and efficient mirrors on a substrate and we report on high- Q , small- V photonic-bandgap microcavities manufactured in ridge waveguides on a silicon-on-insulator wafer. The design issues, which takes into account the vertical cladding asymmetry of the structure (air/Si/SiO₂/Si), rely on Bloch mode engineering concepts [9, 10] and are described in section 2. In contrast to earlier works on related geometries, the mirrors, which are composed of subwavelength holes, are not fully periodic; see figure 4(a) for a quick glance at the structure. The non-periodic section (the taper) consists of a fine-tuning of hole positions and diameters. It implements a gradual change of the transverse mode profile aiming at tapering the guided mode bouncing inside the ridge-defect into the evanescent Bloch mode of the periodic section of the mirror. The tapering process reduces radiation losses at the ridge-mirror interface and modal reflectivities of 0.99995 are predicted by three-dimensional (3D) fully vectorial computational results for tapering lengths of only 1 μm . Experimental results are presented in section 3. For fabrication, we use standard direct-electron-beam-writing and Inductively-Coupled-Plasma-etching techniques developed for the electronics industry. The microcavities, which are manufactured in 520 nm \times 340 nm ridge waveguides, are characterized by in-line transmission measurements. A Q factor of 8900, in agreement with computational results, is obtained at telecommunication wavelengths for a *loaded* cavity with a peak transmission at resonance in excess of 60%. This high- Q value represents a 20-fold improvement over previously reported Q 's for similar geometries [11]–[14] or over a point-defect cavity in a 2D photonic crystal recently manufactured on a SiO₂ substrate [8].

Hereafter, we use a 3D fully vectorial frequency-domain modal method relying on Fourier expansion techniques for the numerical analysis. The Fourier-expansion method [15] is a generalization of the Rigorous Coupled Wave Analysis [16], initially developed for grating analysis, to arbitrary non-periodic structures. In brief, the approach relies on an analytical integration of Maxwell's equations along the longitudinal z -axis of the waveguide and on a supercell approach in the two transverse directions. Perfectly matched layers incorporated as nonlinear coordinate transforms [17] mapping the semi-infinite claddings surrounding the waveguide into a finite segment in the complex plane are used in those directions to carefully handle the far-field radiation and to satisfy the outgoing wave conditions at the supercell boundaries. Since this mapping allows for a cancellation of non-evanescent radiations, the electromagnetic fields are null on the boundaries of the supercell and are thus periodic functions of the transversal coordinates. This allows an accurate calculation of the radiated and guided modes in a Fourier (plane-wave) basis for all waveguide sections, and the integration in the longitudinal z -direction by relating recursively the mode amplitudes in the different sections. The stable and efficient approach used for computing the mirror Bloch modes, which is required for modelling semi-infinite mirrors, is described in [18].

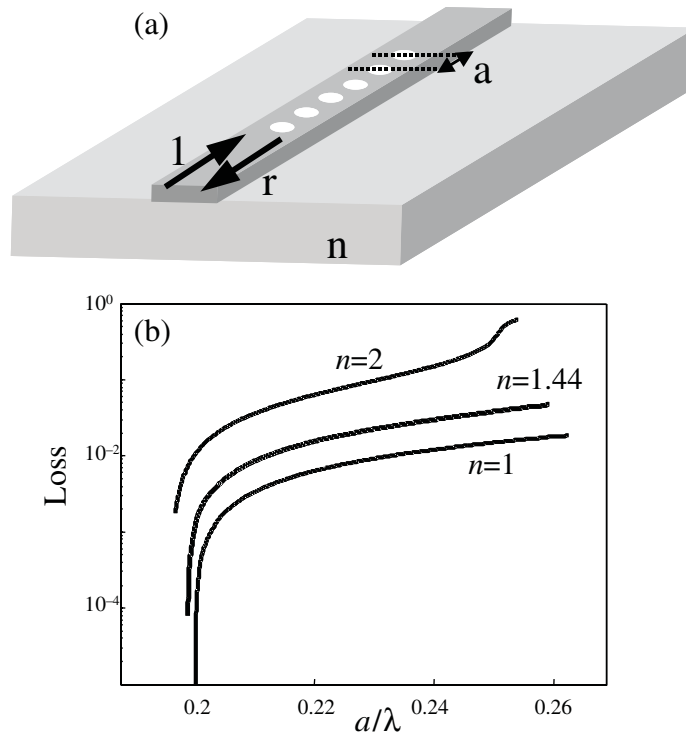


Figure 1. Impact of the substrate refractive index on the modal reflectivity R of a semi-infinite photonic bandgap mirror composed of 180 nm diameter holes. (a) 340 nm thick, 520 nm wide ridge geometry under consideration perforated by holes with 180 nm diameter. (b) Losses ($L = 1 - R$) for different values of the substrate refractive index. The calculations are performed for $\lambda = 1.6 \mu\text{m}$.

2. Design considerations

Throughout the paper, we consider a 340-nm thick, 520 nm wide silicon-ridge waveguide and we assume that the silicon refractive index is 3.48, a value independent of the wavelength; this approximation is largely inessential for the following discussion. At a wavelength of $\lambda = 1.6 \mu\text{m}$, the fundamental TE-like guided mode of the waveguide (denoted M1) has an effective index $n_{\text{eff}} = 2.70$. The waveguide additionally supports a TM-like guided mode ($n_{\text{eff}} = 2.40$) which is not excited at the ridge-mirror interface for symmetry reasons, and a TE-like guided mode (denoted M2) with a small effective index of 1.64. Figure 1(a) illustrates the photonic-bandgap mirror geometry we consider in the following. The mirror is composed of series of equidistant holes (diameter d and periodicity constant a) and is illuminated by the fundamental guided mode M1. Hereafter, we denote by R the modal reflectivity of the semi-infinite fully periodic mirror. R is always smaller than unity, and $L = 1 - R$ represents losses, mainly due to out-of-plane radiation in the claddings. We have noted that a small fraction of the incident light can also be lost by in-plane transmission into the non-evanescent mirror Bloch mode B2 associated to the TE-like guided mode M2. As shown in [19] for GaAs/AlAs pillar microcavities, the existence of a higher-order propagating Bloch mode in a distributed Bragg reflectors can drastically impact the Q factor of a microcavity. However, this effect marginally affects the present discussion and will be omitted in the following.

We first consider the impact of the substrate refractive index (denoted by n) on the modal reflectivity. In figure 1(b), the loss L is displayed in a logarithmic scale as a function of the mirror periodicity a for several values of n , $n = 1$ (air bridge), $n = 1.44$ (SiO₂ substrate) and $n = 2$ (sapphire substrate). The computation is performed for $\lambda = 1.6 \mu\text{m}$. Two trends, which are important for the design of tapered mirrors, are observed. We first note that the amount of radiation losses monolithically increase with the mirror periodicity. This trend is simply understood if one considers that, as the mirror periodicity increases, the non-propagative (evanescent) Bloch mode B1 in the mirror (the mode associated to M1 which is responsible for the reflection) is less and less confined into the silicon ridge and spreads out into the cladding and the holes. Thus the transverse mode-profile mismatch between M1 and B1 becomes more and more severe and radiation losses are largely exalted at the mirror-ridge interface [10]. Very small losses can be obtained for mirrors with small periodicities, i.e. for Bloch modes B1 in the vicinity of the valence-band edge. Although such mirrors guarantee very high reflectivities, they cannot be used in practice because the penetration depth exponentially increases at the band edges and thus many periods are needed to reflect light. The second important trend we observe is that, as the substrate refractive index increases, the loss drastically increases. There are two reasons for this. The first is an increase of the mode profile mismatch between M1 and B1. Indeed as n increases, the centre of mass of B1 shifts down in the substrate more rapidly than that of M1: because of the presence of holes, B1 experiences an average refractive index which is lower than that of M1 and is naturally less confined. Thus, the overlap integral between M1 and B1, which is largely sensitive to centre-of-mass vertical shift [20] is lowered, and radiation losses increase. The second reason results from the leakage of B1 in the substrate. For $n = 2$ and $a/\lambda > 0.25$, B1 is no longer a truly guided mode and some of its Fourier harmonics radiate in the substrate. In our opinion, figure 1 well evidences the conceptual problem related to the design of short high reflectors on a substrate, even for moderate values of n . Let us add that a modal reflectivity of 0.98 as that predicted at midgap frequency for $n = 1.44$ results in a Q factor of only ≈ 700 for single-hole-defect cavities as will be considered hereafter.

In figure 2, we show the impact of the hole diameter on the modal reflectivity R . The computations are performed for $n = 1.44$ and for $\lambda = 1.5 \mu\text{m}$, and the displayed data are restricted to periodicities for which the fundamental mirror Bloch mode B1 is evanescent (bandgap). Two main informations are derived from the figure. Firstly, as in figure 1, we note that very small losses are achieved for small periodicities close to the valence band edge. As mentioned earlier, the associated Bloch modes cannot be used alone to implement a strong reflection. However, since they strongly resemble M1, these Bloch modes offer interesting degrees of freedom for tapering M1 into B1 on short distances [10]. They have been used in the design of the tapered mirror. Secondly, we observe that very high reflectances are achieved only for a narrow range of periodicity in the vicinity of the valence band. The narrower the hole diameter, the wider this range. Targeting a modal reflectivity of 0.9999 for the tapered mirror implies that holes with diameters below 150–170 nm have to be fabricated or that a very highly accurate control of the hole sizes and positions has to be guaranteed by the fabrication process.

The approach used for designing a high-reflectance photonic-bandgap mirror has been described in previous reports [9, 10] and will not be detailed hereafter. We just recall the main aspects. First, we consider a fully periodic mirror with 180 nm hole diameter and a periodicity constant $a = 370$ nm. This mirror offers a ≈ 350 nm wide bandgap centred around $\lambda = 1.55 \mu\text{m}$. In brief, the design consists of reducing the scattering losses involved at the interface between the photonic-bandgap periodic mirrors and the ridge waveguide by introducing a taper (composed

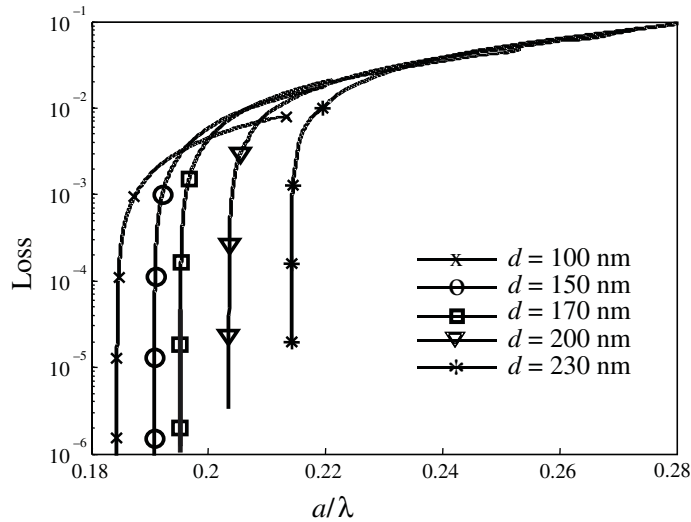


Figure 2. Effect of the hole diameter d on the performance of semi-infinite fully periodic mirrors. The losses $L = 1 - R$ result from radiation losses in the claddings and from in-plane transmission in the mirror Bloch mode B2.

of four hole sections, see figure 4(a)) which aims at implementing a gradual variation of the transverse mode profile between the modes M1 of ridge waveguide and B1 of the mirror. As in previous designs realized for air-bridge ($n = 1$) geometries, the taper sections strongly rely on Bloch modes close to the valence band edge (see figure 2) which offer transverse mode profiles similar to those of M1. More details on the design can be found in the sections relative to figures 4 and 7 in [10].

The scanning electron microscope (SEM) inspections of the fabricated devices, see section 3, have revealed that the holes of the actual devices are accurately positioned but that their diameters are slightly (10–20 nm) smaller than the targeted values. The four tapered holes have diameters of 130, 160, 185 and 181 nm with centre-to-centre hole distances of 300, 315, 325 and 352 nm and the hole diameters in the periodic section of the mirrors are all nearly equal to 181 nm with a periodicity constant $a = 370$ nm. In order to predict the device performance, we have performed 3D computations of the modal reflectivity R of the taper mirror (assuming that the periodic part of the mirrors is semi-infinite, $N = \infty$) for *the geometric parameters actually measured on the device*. Figure 3 compares the calculated loss ($1 - R$) spectrum of the tapered mirror (circles) with that of the fully periodic mirror (squares). Clearly, the taper drastically reduces the losses at the mirror/ridge interface, despite the difference between the targeted and actual hole-diameter values. This evidences the robustness of the tapering process to fabrication errors. At midgap frequency ($\lambda \approx 1.6 \mu\text{m}$), the losses are very small, $1 - R = 5 \times 10^{-5}$. This implies that the progressive mode conversion from M1 to B1 not only suppresses the out-of-plane radiation, but also results in a very weak in-plane excitation of B2. Additionally, let us note that the loss spectra of the tapered and fully periodic mirrors largely differ. The monotonic decay observed for the periodic mirror does not show up in the tapered structure which rather presents a dip at $\lambda = 1.6 \mu\text{m}$. A similar loss-spectrum behaviour was also obtained for the designed taper. It is a direct and general consequence of the design itself, which uses Bloch modes close to

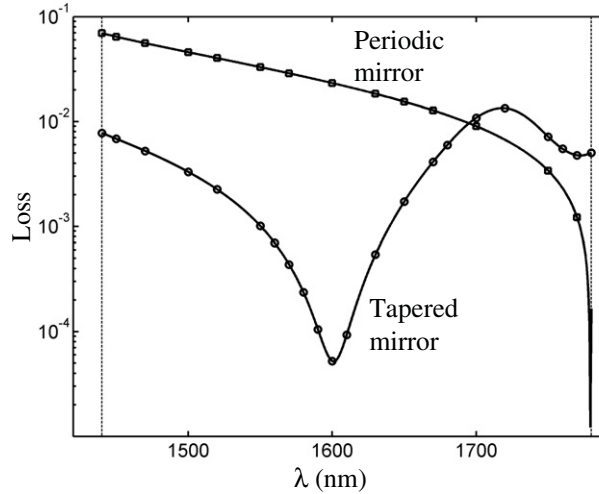


Figure 3. Comparison between a periodic and a tapered photonic-bandgap mirror. Circles (resp. squares) correspond to losses ($L = 1 - R$) for tapered (resp. periodic) semi-infinite mirrors ($N = \infty$). The vertical thin lines indicate the band edges of the periodic mirror. The calculation is performed for the geometric parameters actually measured on the sample: tapered holes have diameters of 130, 160, 185 and 181 nm with centre-to-centre hole distances of 300, 315, 325 and 352 nm. The periodic ($a = 370$ nm) mirrors are composed of holes with a 181 nm diameter.

the valence band edge. As the wavelength departs from the nominal wavelength value used for the design, these Bloch modes cease to resemble M1 and the transverse-mode-profile mismatch between M1 and the Bloch modes involved in the four-hole tapered section is enhanced. Thus losses increase. Finally, we note that the tapering process is relatively broadband. The losses are maintained below 10^{-4} (resp. 10^{-3}) over a 20 nm (resp. 100 nm) large spectral interval.

Using a Fabry-Perot model [7], the Q factor of a cavity formed by the association of two identical mirrors with reflectivity R reads as

$$Q = \frac{\pi}{1 - R} \left[2 \frac{L}{\lambda_0} n_g - \frac{\lambda_0}{\pi} \left(\frac{\partial \varphi}{\partial \lambda} \right)_{\lambda_0} \right], \quad (1)$$

where n_g is the group index of M1, L the cavity defect length (side-to-side separation distance between the two smaller holes) and φ the phase of the modal reflectivity coefficient, $r = R^{1/2} \exp(i\varphi)$. From equation (1), we predict that a nanocavity formed by the association of two tapered semi-infinite mirrors should exhibit an intrinsic Q value of 380000 at $\lambda = 1.6$. Finally, let us mention that the tapered sections solely involve evanescent Bloch modes [9], and thus not only provide a transverse-mode profile conversion, but also reflects light. As a consequence, a strong light confinement is achieved. The corresponding calculated cavity mode volume is $V \approx 0.6(\lambda/n)^3$.

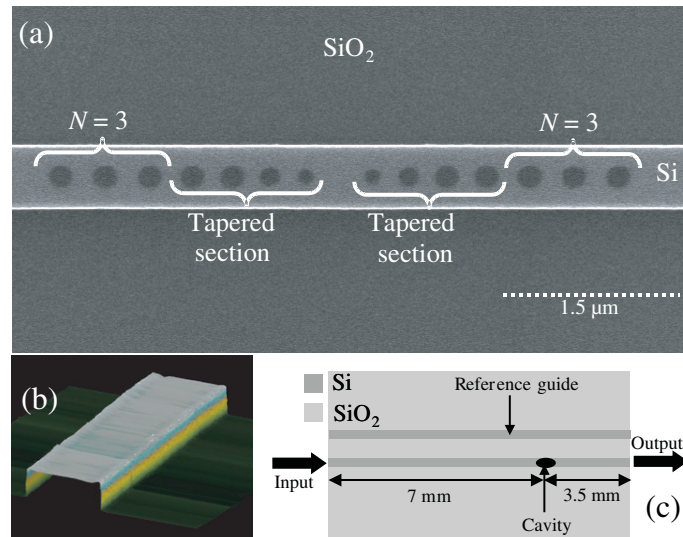


Figure 4. (a) Scanning electron micrograph of a fabricated microcavity. Each photonic-bandgap mirror is composed of a four-hole taper and a periodic section with N holes ($N = 3$ in the photograph). (b) 3D AFM picture of the ridge waveguide. (c) Sketch of the entire ridge-access geometry used for transmission measurements of the cavity.

3. Experimental results

Several series of cavities with $N = 1, 2, \dots, 4$ and different defect lengths L are fabricated using Soitec silicon-on-insulator wafers with a 340 nm Si-core thickness and a 2 μm thick SiO₂ buried spacer. The ridge and hole patterning is performed by electron-beam lithography with a Leica VB-6UHR vector scan generator on a single 400 nm thick NEB22 negative resist designed by SUMITOMO and spin coated on top of the sample. The electron beam energy is 100 keV resulting in a 5 nm probe-beam diameter. After developing the resist, Inductively-Coupled-Plasma etching of the sample is performed in an inductively coupled industrial plasma chamber (DPS from Applied Materials Inc). The native oxide is first removed by a short breakthrough with a CF₄ gas mixture. The silicon native layer is then etched with a Cl₂/HBr/O₂ gas mixture, at a pressure of 4 mT with a source power of 350 W and a bias power of 120 W. Finally, resist is stripped by oxygen plasma. The silicon etching rate is typically 150 nm min⁻¹ and the silicon dioxide cladding is used as an etch stop. Then, the wafer is manually cleaved to obtain optical facets. Figure 4(a) shows an SEM picture of a cavity formed by a defect surrounded by two identical mirrors with $N = 3$ holes in the periodic mirror. The ridge width is 520 nm and typical hole diameters vary from 130 to 190 nm. The whole layout, see figure 4(c), incorporates a few millimetre long access waveguide.

After fabrication, the cavities are first observed with an SEM and an atomic force microscope (AFM). An SEM picture of a microcavity is shown in figure 4(a). From the AFM observations, see figure 4(b), we infer that the surface roughness of the ridge sidewalls is approximately 3 nm rms. The device under test is mounted on a XYZ translational stage. TE-polarized light from a broadband LED source with a bandwidth spanning 1200–1700 nm is launched into the 7 mm long access-waveguide using a $\times 36$ microscope objective. This first experiment allows for a

broadband scan of the transmission spectrum and for a qualitative determination of the spectral position of the resonance. Then for quantitative analysis, light from a high-resolution tunable external laser source (1450–1600 nm) is coupled to the device via a polarization maintaining microlensed fibre. The fibre tip produces a spot with a beam waist of $\approx 2.1 \mu\text{m}$ with minimal mixing of TE-TM modes (rejection ratio of over 20–30 dB). After passing through the device, the light is collected by a high-magnification imaging system composed of a $\times 20$ microscope objective (NA = 0.30) and of AR coated plano-convex lens with a 50 mm focal length. The waveguide output is imaged either onto an IR camera for observing light at the output cleaved facet or onto an InGaAs photodiode for quantitative transmission measurements. Additionally, when using the InGaAs photodiode, the imaging system incorporates a $100 \mu\text{m}$ pinhole and a polarizer in order to spatially filter inevitable spurious substrate-guided light.

We first estimate the attenuation loss of the ridge waveguides. Ten reference waveguides, without cavities and with two different lengths of 6.5 and 10.2 mm, are characterized by measuring the contrasts of the Fabry-Perot fringes resulting from the bouncing of light between the cleaved facets. Assuming a facet modal reflectivity of 0.36, a value calculated with the Fourier modal method, we obtain a straight-waveguide-attenuation loss of $6 \pm 1 \text{ dB cm}^{-1}$. This value is compatible with the sidewall roughness measured with the AFM [21], and is only twice as large as the best attenuation reported so far for similar SOI ridge geometries [22] with very strong confinements.

The most important results obtained for transmission measurements of cavities with defect length $L = 425 \text{ nm}$ are summarized in figure 5. Figures 5(a)–(d) are obtained with the broadband source and the laser, respectively, and for different cavities. Figure 5(a) represents the transmission spectrum of the cavity with $N = 4$, obtained with the white source. It shows a broad bandgap and a resonance peak located at $\lambda \approx 1.58 \mu\text{m}$, marked by a vertical arrow. The data are normalized by transmission measurements performed for an identical reference waveguide which is located at a few microns aside. These measurements do not allow for a determination of the resonance linewidth that is convolved by the finite spectral resolution of the spectrum analyser apparatus.

To avoid this limitation, we perform transmission measurements with the laser source. The results (in arbitrary units) are shown in figures 5(b)–(d) for cavities with $N = 2, 3$ and 4. The high-frequency oscillations in the experimental spectra are Fabry-Perot fringes due to the bouncing of light between the cleaved facets of the access-ridge waveguides. After filtering by a low-pass filter, the bold curves are obtained from the measured data and the Q values are estimated by fitting with Fabry-Perot Airy-functions. Table 1 compares the measured and calculated Q values. The computed Q values are obtained using equation (1) for a resonance wavelength of $\lambda = 1.6 \mu\text{m}$. The bracketed term in the right-hand side of equation (1) is equal to 19.6, for a group-index of $n_g = 4.12$ and for a cavity geometrical length (side-to-side inner hole distance) of $L = 425 \text{ nm}$, and the modal reflectivity for $N = 2, 3$ and 4 is computed with the Fourier modal method. As evidenced by table 1, the computed values, Q_c , are in good agreement with the experimental results, Q_e . Note that the 7 nm maximum resonance wavelength shift between the nominal resonance value of $1.6 \mu\text{m}$ and the measured ones are well within the accuracy of the SEM technique used to determine the hole sizes; as we checked, the calculated Q_c values do not depend on this slight shift because the cavities' Q 's of the fabricated devices are limited by the in-plane mirror transmission and not by radiation losses in the claddings. The largest measured Q factor is 8900; this represents a 20-fold improvement over previously reported Q 's for similar geometries. Another measure of cavity perfection that does not include propagation

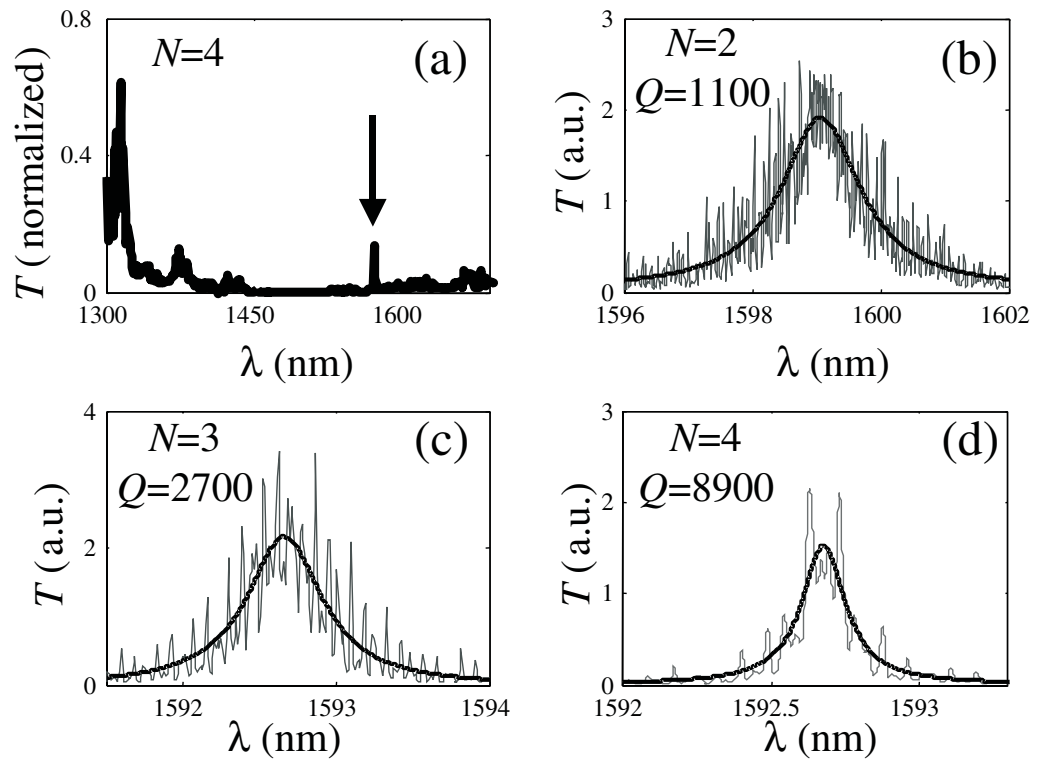


Figure 5. Transmission spectra obtained for different cavities. (a) Transmission spectrum obtained with a broadband white source for the cavity with $N = 4$. For the sake of normalization, the measured transmitted power is divided by that of an identical ridge waveguide without cavity. The peak transmission at resonance ($\lambda \approx 1.6 \mu\text{m}$) is ≈ 0.18 . (b)–(d) Transmission spectra obtained with the Tunics laser for microcavities with $N = 2, 3$ and 4 . Plots are provided in arbitrary units.

Table 1. Comparison between the calculated and measured Q values.

N	2	3	4	∞
Q	1100	2700	8900	
Q_c	1270	3200	9600	400000

effects within the cavity as does the Q factor, is the cavity finesse $F = \pi/(1 - R)$. For $N = 4$, F is as high as 1400.

The peak-transmission T_{max} at resonance is another important figure of merit of cavities. Its estimation is challenging. In the white source experiment (see figure 5(a)), a T_{max} value of ≈ 0.18 is measured. As mentioned before, the resonance peak obtained with the white lamp is not resolved by the spectrum analyser, and we believe that the actual value is much larger. In general, for a Fabry-Perot cavity, one expects that

$$T_{\text{max}} = (1 + L/T)^{-2}, \quad (2)$$

where T is the mirror modal transmission, and $L = 1 - R - T$ is the mirror loss (mainly radiation into the cladding in the present case). In the measurements performed with the laser source (figures 5(b)–(d) in arbitrary unit) for tapered cavities with $N = 2, 3$ and 4, we do not observe any significant trend showing a decrease of T_{\max} with N , the slightly smaller value obtained for $N = 4$ in figure 5(d) being well within the uncertainty of repeatability of the injection into the cleaved facet. In other words, the mode lifetime of the cavity with $N = 4$ is likely to be limited by in-plane-transmission, rather than radiation loss ($T > L$). To check this, we have recorded several times the transmission spectra of the reference waveguide and of the $N = 4$ cavity, systematically realigning the microlensed fibre with the waveguide input facets before recording. From these spectra, we estimate that the peak transmission for the $N = 4$ cavity is larger than 0.6. Note that the corresponding calculated T_{\max} value at $\lambda = 1.6 \mu\text{m}$ is larger than 0.99. From equation (2), a T_{\max} value of 0.6 implies that $T = 3.4L$. Thus the intrinsic Q value of the fabricated device, $Q = 19.6/L$, is expected to be larger than 40000, a value 10 times smaller than the theoretical value (see table 1).

4. Conclusion

The properties of ultra-small microcavities formed by a pair of photonic-bandgap mirrors in a ridge waveguide on a low-refractive index substrate have been studied. Despite the presence of a dissymmetric Air/SiO₂ cladding, we have shown theoretically that μm -long mirrors with very high reflectance (modal reflectivity >0.9999) over a 20 nm spectral range can be designed by incorporating tapers into the mirror. The designed devices have been fabricated in a silicon-on-insulator wafer with electron-beam lithography and Inductive-Coupled-Plasma etching for operation at telecommunication wavelengths. A Q factor of 8900 along with a peak transmission larger than 0.6 have been measured for microcavities incorporating mirrors with typical hole diameters varying from 130 to 190 nm in the taper. The Q value which is limited by the mirror transmission and not by the radiation losses is in agreement with the (loaded) Q of 9600 calculated for the geometric parameters measured on the actual samples. To our knowledge, the measured Q value is two orders of magnitude larger than that achieved in previous reports for cavities with similar mode volumes on a substrate [8], [11]–[14]. An intrinsic Q factor larger than 40000, a value 10 times smaller than that predicted theoretically, is anticipated for the actual device if one removes the in-plane coupling effect with the access waveguides.

In contrast to previous works based on photonic-bandgap microcavities in suspended membranes, the present cavities possess strong mechanical robustness, thus making them attractive from the viewpoint of integration in large systems. In addition, we anticipate that the encapsulation of the cavity in silicon dioxide upper-cladding which is vital for practical applications [23], would have a beneficial impact of the cavity performance, since symmetric cladding offer lower radiation losses in comparison to dissymmetric ones. Such high- Q nanocavities could be applied across various fields of engineering, including nano-lasers [24] and photonic modulators [25] for instance. The measured Q value is fully compatible with bandwidth requirements needed for WDM applications. Additionally, by use of other materials like GaAs for instance, similar microcavities may as well be used for studying quantum electrodynamics effects. Note that the recent observation [26] of the strong coupling regime has been achieved with a $1.5 \mu\text{m}$ diameter micropillar geometry, offering a Q factor equal to that reported in the present, but with a mode volume ≈ 30 times larger.

Acknowledgments

CEA-LETI is acknowledged for the access to the micro/nanofabrication facilities. This work is supported by the Miraman ANR2006 project. PV acknowledges support from CNRS and CEA for his PhD fellowship. The authors acknowledge Jérôme Thiault for the AFM characterization.

References

- [1] Little B E and Chu S T 2000 Toward very large-scale integrated photonics *Opt. Photonics News* 24–29, November 2000
- [2] Vahala K J 2003 Optical microcavities *Nature* **424** 839
- [3] Yokoyama H and Ujihara K 1996 *Spontaneous Emission and Laser Oscillation in Microcavities* (Boca Raton, FL: CRC Press)
- [4] Kippenberg T J, Spillane S M and Vahala K J 2004 Demonstration of ultra-high-Q small mode volume toroid microcavities on a chip *Appl. Phys. Lett.* **85** 6113–5
- [5] Varoutsis S, Laurent S, Sagnes I, Lemaitre A, Ferlazzo L, Meriadec C, Patriarche G, Robert-Philip I and Abram I 2005 Reactive-ion etching of high-Q and submicron-diameter GaAs/AlAs micropillar cavities *J. Vac. Sci. Technol. B* **23** 2499–503
- [6] Kuramochi E, Notomi M, Mitsugi S, Shinya A and Tanabe T 2006 Ultrahigh-Q photonic crystal nanocavities realized by the local width modulation of a line defect *Appl. Phys. Lett.* **88** 041112
- [7] Sauvan C, Lalanne P and Hugonin J P 2005 Slow-wave effect and mode-profile matching in photonic crystal microcavities *Phys. Rev. B* **71** 165118
- [8] Tanaka Y, Asano T, Hatsuta R and Noda S 2006 Investigation of point-defect cavity formed in two-dimensional photonic crystal slab with one-sided dielectric cladding *Appl. Phys. Lett.* **88** 011112
- [9] Lalanne P and Hugonin J P 2003 Bloch-wave engineering for high Q's, small V's microcavities *IEEE J. Quantum Electron.* **39** 1430–8
- [10] Sauvan C, Lecamp G, Lalanne P and Hugonin J P 2005 Modal-reflectivity enhancement by geometry tuning in photonic crystal microcavities *Opt. Express* **13** 245–55
- [11] Zhang J P, Chu D Y, Wu S L, Bi W G, Tiberio R C, Joseph R M, Taflove A, Tu C W and Ho S T 1996 *IEEE Photon. Technol. Lett.* **8** 491
- [12] Ripin D J, Lim K Y, Petrich G S, Villeneuve P R, Fan S, Thoen E R, Joannopoulos J D, Ippen E P and Kolodziejcki L A 2000 Photonic band gap airbridge microcavity resonances in GaAs/AlxOy waveguides *J. Appl. Phys.* **87** 1578
- [13] Jugessur A S, Pottier P and De La Rue R M 2003 One-dimensional periodic photonic crystal microcavity filters with transition mode-matching features, embedded in ridge waveguides *Electron. Lett.* **39** 367–9
- [14] Foresi J S, Villeneuve P R, Ferrera J, Thoen E R, Steinmeyer G, Fan S, Joannopoulos J D, Kimerling L C, Smith H I and Ippen E P 1997 Photonic-bandgap microcavities in optical waveguides *Nature* **390** 143–5
- [15] Silberstein E, Lalanne P, Hugonin J P and Cao Q 2001 On the use of grating theory in integrated optics *J. Opt. Soc. Am. A* **18** 2865–75
- [16] Moharam M G, Grann E B, Pommet D A and Gaylord T K 1995 Formulation for stable and efficient implementation of the rigorous coupled-wave analysis of binary gratings *J. Opt. Soc. Am. A* **12** 1068–76
- [17] Hugonin J P and Lalanne P 2005 Perfectly-matched-layers as nonlinear coordinate transforms: a generalized formalization *J. Opt. Soc. Am. A* **22** 1844–9
- [18] Cao Q, Lalanne P and Hugonin J P 2002 Stable and efficient Bloch-mode computational method for one-dimensional grating waveguide *J. Opt. Soc. Am. A* **19** 335–8
- [19] Lecamp G, Lalanne P, Hugonin J P and Gérard J M 2005 Energy transfer through laterally confined Bragg mirrors and its impact on pillar microcavities *IEEE J. Quantum Electron.* **41** 1323–9

- [20] Palamaru M and Lalanne P 2001 Photonic crystal waveguides: out-of-plane losses and adiabatic modal conversion *Appl. Phys. Lett.* **78** 1466–9
- [21] Lardenois S, Pascal D, Vivien L, Cassan E, Laval S, Orobtcouk R, Heitzmann M, Bouzaida N and Mollard L 2003 Low-loss submicrometer silicon-on-insulator rib waveguides and corner mirrors *Opt. Lett.* **28** 1150–2
- [22] Vlasov Y A and McNab S J 2004 Losses in single-mode silicon-on-insulator strip waveguides and bends *Opt. Express* **12** 1622–31
- [23] Marki I, Salt M, Herzig H P, Stanley R, Melhaoui E L, Lyan P and Fedeli J M 2005 Characterization of buried photonic crystal waveguides and microcavities fabricated by deep ultraviolet lithography *J. Appl. Phys.* **98** 013103
- [24] Zhang J P, Chu D Y, Wu S L, Ho S T, Bi W G, Tu C W and Tiberio R C 1995 Photonic wire laser *Phys. Rev. Lett.* **75** 2678–81
- [25] Gardes F Y, Reed G T, Emerson N G and Png C E 2005 A sub-micron depletion-type photonic modulator in silicon on insulator *Opt. Express* **13** 8845–54
- [26] Reithmaier J P, Sek G, Löffler A, Hofmann C, Kuhn S, Reitzenstein S, Keldysh L V, Kulakovskii V D, Reinecke T L and Forchel A 2004 Strong coupling in a single quantum dot–semiconductor microcavity system *Nature* **432** 197–200